Advances in Energy and Materials Research
https://jaem.qom.ac.ir/

Hydrothermal Synthesis of Ce-Doped CdS Nanomaterials for Visible-Light Photocatalytic Applications in Energy and Environmental Systems

Younes Hanifehpour [1]* and Mohammadreza Rezaei [1]

[1]*Department of Chemistry, Sayyed Jamaleddin Asadabadi University, Asadabad, Iran*
** Corresponding author. hanifehpour@sjau.ac.ir*

Article Info

Article type:
Research Article

Article history:
Received 18 Jan 2025
Received in revised form 20 Mar 2025
Accepted 15 May 2025
Published online 25 Jun 2025

Keywords:
Photocatalysis; Cerium; Nanoparticles; RB 19; Hydrothermal.

ABSTRACT

CexCd1–xS ($0 \leq x \leq 0.08$) nanoparticles with varying cerium doping levels were successfully synthesized via a hydrothermal method. The structural, morphological, compositional, and optical properties of the prepared samples were systematically characterized using X-ray diffraction (XRD), scanning electron microscopy (SEM), energy-dispersive X-ray spectroscopy (EDX), X-ray photoelectron spectroscopy (XPS), and UV–Vis diffuse reflectance spectroscopy (DRS). The photocatalytic activity of pure and Ce-doped CdS nanoparticles was evaluated through the visible-light-driven decolorization of Reactive Blue 19 in aqueous solution. Among the investigated compositions, the sample containing 6% Ce exhibited the highest photocatalytic efficiency compared to other dopant concentrations. The effects of key operational parameters—including cerium content, catalyst dosage, initial dye concentration, and the presence of radical scavengers—were systematically examined. The addition of radical scavengers such as iodide, carbonate, sulfite, and 1,4-benzoquinone significantly suppressed the decolorization efficiency, indicating the crucial role of reactive species in the degradation process. Overall, the results demonstrate that Ce-doped CdS nanoparticles, particularly at an optimal doping level of 6%, exhibit enhanced visible-light photocatalytic performance and promising reusability, highlighting their potential application in the removal of organic pollutants from wastewater.

Cite this article: Hanifehpour, Y., & Rezaei, M. (2025). Hydrothermal Synthesis of Ce-Doped CdS Nanomaterials for Visible-Light Photocatalytic Applications in Energy and Environmental Systems. Advances in Energy and Materials Research, 2(6), , 4-11.
https://doi.org/10.22091/jaem.2026.15160.1038

DOI: 10.22091/jaem.2026.15160.1038
Publisher: University of Qom.

1. Introduction

Recently, rapid industrial development operations have resulted in the release of significant quantities of wastewater filled with various pollutants, which poses environmental and health risks and other living beings. Effluents containing dye produced by textile industries are major contaminants in wastewater, causing significant issues due to their persistence in color and high COD loading in the water. To address this issue, along with several other proven methods, the approach utilizing semiconductor photocatalysts presents a promising solution for degrading organic contaminants in wastewater [1-4]. Photocatalysis is a process in which a semiconductor material captures light with energy equal to or exceeding its band gap, leading to excitations of valence band electrons into the conduction band. Charge separation results in the creation of electron-hole pairs that can subsequently produce free radicals within the system for substrate redox reactions. The free radicals produced, like hydroxyl (•OH), are highly effective at oxidizing organic substances and can break down pollutants [5-8]. CdS is considered an effective semiconductor under visible light irradiation because of its low band gap and the swift creation of electron-hole pairs (charge carriers) through photoexcitation. Cadmium sulfide nanowires demonstrated remarkable catalytic degradation performance in both the UV and visible spectrum [9-11]. Salimi et al. have reported one-dimensional CdS NWs combined with TiO_2 nanoparticles, demonstrating high-performance photocatalytic activity for the degradation of methyl orange (MO), methylene blue (MB), and rhodamine B (Rh B) when exposed to visible and sunlight irradiation [12]. In this study, a simple hydrothermal route has been introduced to the synthesis of Ce-doped CdS nanoparticles. Also, the photocatalytic activity of synthesized Ce-doped CdS nanoparticles was investigated towards RB 19 (as a model organic dye) decolorization under visible light irradiation. Other objectives of this work are to investigate the effect of inorganic ions on the decolorization efficiency of RB 19.

2. Experimental sections

2.1. Chemicals and materials

All chemicals used in this study were of analytical grade and were used without further purification. $N_2H_4.H2O$ (99 %), Cd $(NO_3)_2.4H_2O$ (99.5 %), S (99 %) and NaOH were obtained from Merck; Ce $(NO_3)_3 \cdot 6$ H_2O and ethanol (99 %) were obtained from Sigma-Aldrich. Reactive Blue 19 was purchased from Shimi Boyakhsaz (Iran) and used without further purification. The characteristic of this dye is presented in Table 1.

Table 1. The characteristics of RB 19

Chemical structure	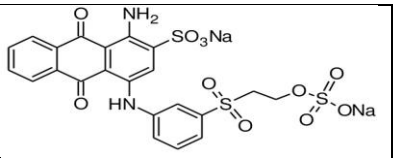
Color index name	Reactive Blue 19
Molecular formula	$C_{22}H_{16}N_2Na_2O_{11}S_3$
λ_{max} (nm)	501
M_w (g/mol)	626.54

2.2. Synthesis of $Ce_xCd_{1-x}S$ nanoparticles

Ce-doped CdS nanoparticles with variable Ce contents (0–8 mol %) were prepared using a hydrothermal method and hydrazine hydrate ($N_2H_4.H_2O$) as the reducing agent. In a standard synthesis, 2 mmol of S powder and 3 mmol of NaOH, along with suitable molar ratios of Ce $(NO_3)_3$ • 6 H_2O and Cd $(NO_3)_2$ • 4 H_2O, were initially dissolved in 40 mL of distilled water. The solution was stirred at 150 rpm, hydrazine hydrate ($N_2H_4.H2O$) was subsequently added gradually to the solution mentioned above. The resulting mixture was transferred into a 50 mL stainless-steel autoclave lined with Teflon, which was then sealed and placed in an oven at 160 °C for 24 hours, after which the autoclave was permitted to cool to room temperature naturally. $Ce_xCd_{1-x}S$ nanoparticles, as-synthesized, were gathered and rinsed multiple times with distilled water and absolute ethanol to eliminate remaining impurities, then vacuum dried at 50 °C for 3 hours. Ultimately, a dark yellow powder was produced.

2.3. Characterization

To assess the crystal phase composition of the synthesized CdS and Ce-doped CdS samples, XRD characterization was performed at room temperature using a D8 Advance diffractometer from Bruker, Germany, utilizing monochromatic high-intensity Cu Ka radiation (λ =1.5406 A°), with an accelerating voltage of 40 kV and an emission current of 30 mA. Elemental analyses were performed utilizing a connected ISIS300 and an Oxford EDS (energy dispersive spectroscopy) detector. The structure of materials was analyzed using a scanning electron microscope SEM (Hitachi S-4200, Japan).

2.4. Photocatalytic activity and experimental procedures

The photocatalytic activity of pure and Ce-doped CdS nanoparticles was evaluated by the decolorization of RB 19 in an aqueous solution under visible light. In a typical process, 0.1 g of the photocatalyst powder was added into 100 mL RB 19 solution with an initial concentration of 25 mg/L. The pH of samples was adjusted by using H_2SO_4 and NaOH aqueous solutions.

The suspension of photocatalyst and RB 19 was magnetically stirred in a quartz photoreactor in the dark for 20 min to establish an adsorption/desorption equilibrium of the dye. Then, the solution was irradiated by a 40W fluorescent visible lamp (GK-140, Iran) as the light source for a set irradiation time. Light irradiated from compact 40W fluorescent visible lamp was passed from cutoff filter for providing visible light illumination (λ>420 nm). The measured light intensity at the distance of 15 cm from lamp (distance between lamp and surface of solution) was 4250 lux. Visible light irradiation of the reactor was performed for 20, 40, 60, 80 and 120 min. Samples were withdrawn regularly from the reactor, and dispersed powders were removed in a centrifuge. The color removal was evaluated by determining its absorbance at λ_{max}= 501 nm by using UV–Vis spectrophotometer, Lightwave S2000 (England). The decolorization efficiency was calculated using eq 1:

Decolorizatoin efficiency (%) = [1- (C / C_0)] * 100 (1)

where Co and C are the initial and final concentration of the dye in the solution (mg/L), respectively [13-15]. It must be mentioned that the photocatalytic performance of $Ce_xCd_{1-x}S$ nanoparticles in the pH range of 4 to10 was evaluated and we found the maximum photocatalytic activity at pH=5.

3. Results and discussion

3.1. Characterization of the synthesized samples

Figure 1 shows XRD patterns of 8% Ce doped CdS sample. The XRD pattern of Ce-doped CdS powders shows peaks which can be indexed to (100), (002), (101), (102), (110), (103), (200), (112), (201), (004), (202), (203), (210), (211), (114) and (105) planes . All the diffraction peaks of the samples can be readily indexed to the pure typical well-crystallized hexagonal CdS (JCPDS No. 10-0454) [16, 17]. No peak for impurities was detected, confirming that the applied hydrothermal method in this study was successful in synthesizing the samples.

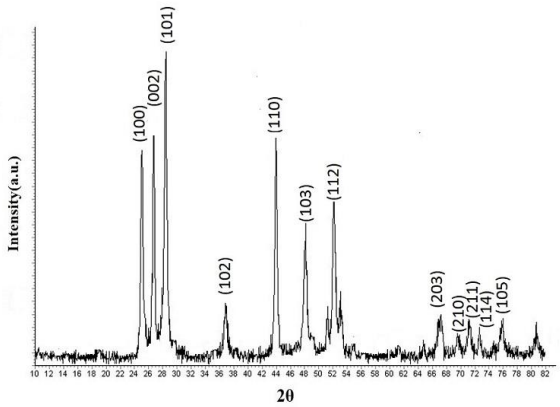

Fig. 1. Powder X-ray diffraction pattern of $Ce_{0.08}Cd_{0.92}S$ synthesized at 160 °C and 24 h.

In order to further clarify the size and shape of the nanoparticles, SEM image were obtained at different magnifications. Figures 2 shows the SEM microphotographs of the CdS and 8 % Ce doped CdS samples, respectively. In figure 2a, uniform and spherical nanoparticles of about 15-60 nm in diameter with a little agglomeration can be seen. In Figure 2b, very uniform and spherical shaped Ce doped CdS nanoparticles can be observed. The diameter of these particles is around 30-80 nm which is bigger than that of undoped CdS nanoparticles. The particle size distribution of as-prepared compound is seen at figure 3 and confirms the SEM results. These figures confirm that doping of Ce^{3+} into the structure of CdS does not change the morphology of CdS nanoparticles.

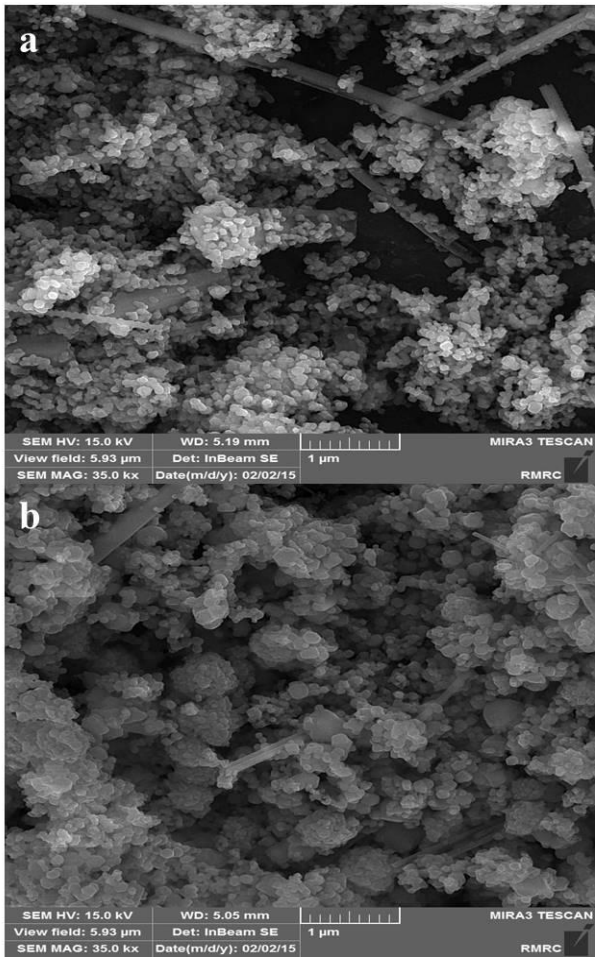

Fig. 2 SEM image of (a) CdS and $Ce_{0.08}Cd_{0.92}S$ nanoparticles synthesized at 160 °C and 24 h.

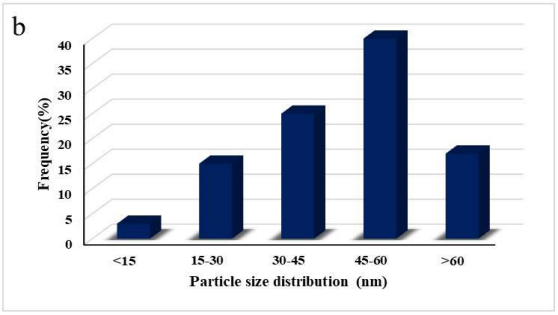

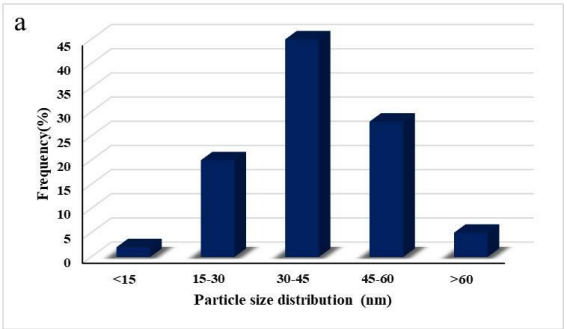

Figure 3. Size distribution of (a) pure CdS and (b) 8 %Ce-doped CdS nanoparticles.

The chemical compositions of CdS nanoparticles were analyzed using EDX to verify the purity of the products. The EDX patterns for the nanoparticles are displayed in Figures 4 and 5. The findings confirm the nanomaterials' elevated purity. The EDX spectra of CdS nanoparticles in Fig. 4 reveal the presence of key chemical elements, specifically Cd and S. The elemental composition derived from EDX analysis for CdS was 49.48 and 50.52 mol % of CdS, which further validates the existence of CdS. The EDX spectra of Ce-doped CdS nanoparticles in Fig. 5 reveal the presence of primary chemical elements, specifically Cd, S, and Ce. The elemental makeup derived from EDX analysis for 8% Ce-doped CdS was 44.34, 49.33, and 6.33 mol% of Cd, S, and Ce, respectively, which further verifies that most of the ions are Ce^{+3} doped into CdS.

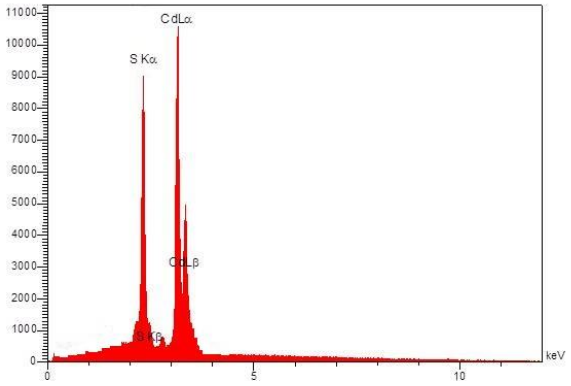

Figure 4. EDX pattern of CdS nanoparticles.

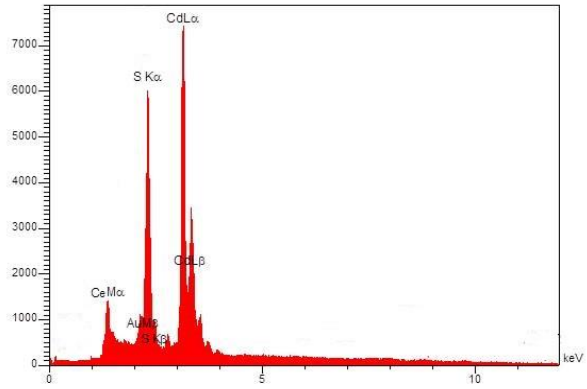

Figure 5. EDX pattern of $Ce_{0.08}Cd_{0.92}S$ nanoparticles.

3.2. The effect of operating conditions on the photocatalysis of RB 19

3.2.1. Effect of Ce^{3+} content of $Ce_xCd_{1-x}S$ nanoparticles

To achieve the best conditions for photocatalytic activity, the degradation of RB 19 was examined with $Ce_xCd_{1-x}S$ at varying mole fractions (x = 0.00, 0.04,

0.08) under visible light exposure. Figure 6 illustrates the decolorization efficiency of RB 19 using various Ce-doped CdS photocatalysts throughout a 120-minute reaction period. Figure 6 clearly shows that the samples infused with the correct amount of Ce ion demonstrated significantly greater photocatalytic activity than pure CdS, particularly the sample with a 0.06 molar ratio of Ce, which displayed the highest photocatalytic activity. With low mole fractions of dopant, Ce^{3+} ions can trap photoinduced electrons, slowing down the electron/hole recombination rate, which subsequently improves the interfacial charge transfer for RB 19 degradation [18, 19]. Moreover, cerium can exist as Ce^{3+} and Ce^{4+}. Thus, Ce^{3+} may give an electron to O_2 adsorbed on the surface of Ce-doped CdS to form $^{\bullet}O_2^-$ by transforming into Ce^{4+}, favoring a charged migration to O_2 and an enhancement of the photoreaction rate in comparison with that of pure CdS. On the other hand, the Ce^{4+} species may receive photogenerated electrons in the conduction band of CdS to form Ce^{3+} (eq 2-5). These reactions are the reason for enhanced photoactivity of CdS.

$$Ce^{3+} + O_2 \rightarrow Ce^{4+} + {}^{\bullet}O_2^- \quad (2)$$

$$Ce^{4+} + e^- \rightarrow Ce^{3+} \quad (3)$$

$$^{\bullet}O_2^- + H^+ \rightarrow {}^{\bullet}O_2H \quad (4)$$

$$2\,{}^{\bullet}O_2H \rightarrow H_2O_2 + O_2 \quad (5)$$

Both the $OH^{\bullet}$ and $^{\bullet}O_2^-$ radicals together with H_2O_2 are excellent oxidants for degradation of organic compounds. Among different Ce-doped CdS nanoparticles, the application of 6% Ce-doped nanoparticles led to the highest decolorization efficiency (83.29%).

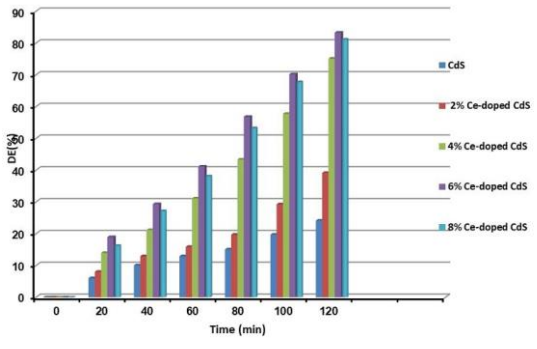

Figure 6. The effect of Ce^{3+} dopant content on the decolorization of 25 mg/L RB 19 (catalyst loading 0.1 g/L)

It has been established that incorporating the right quantity of doping element can be essential for attaining elevated photocatalytic activity [20, 21]. Elevating the concentration of Ce in the catalyst's structure caused an increased surface barrier and a narrower space charge region, facilitating effective separation of the generated electron−hole pairs. Raising the cerium concentration to a certain level leads to surpassing the space charge layer by enhancing the penetration depth of visible light in CdS nanoparticles. This simplifies the recombination of electron−hole pairs, resulting in reduced photocatalytic decolorization efficiency. Moreover, the surplus dopant on the surface of CdS nanoparticles results in reduced photocatalytic performance of the photocatalyst because of an increased number of electron-hole recombination sites .Based on the results obtained 6% Ce-doped CdS nanoparticles were utilized for conducting the remaining experiments.

The changes in the UV–Vis absorption spectra of RB 19 during the photocatalytic process at different irradiation times are shown in Fig. 7. The decreasing concentration of RB 19 during the photocatalytic reaction is used to evaluate the activity of photocatalyst.

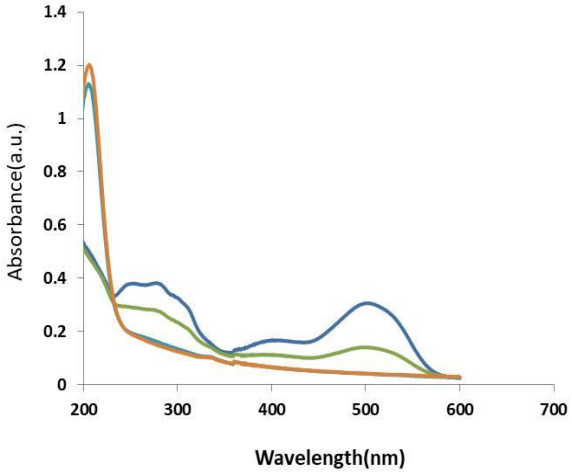

Figure 7. Degradation of RB 19 under visible light irradiation using $Ce_{0.06}Cd_{0.94}S$ nanoparticles.

3.2.3. Effect of Catalyst Dosage

To assess the influence of catalyst dosage on decolorization efficiency, the amount of catalyst was altered between 0.25 and 2 g/L, with the results shown in Figure 8. In this series of experiments, both reaction time and initial dye concentration remained constant at 120 minutes and 25 mg/L, respectively. Figure 8 illustrates that at catalyst concentrations of 0.25, 0.5, 0.75, 1, and 2 g/L, the decolorization efficiencies were 57.71, 61.23, 69.22, 83.29, and 80.12 %, respectively. Therefore, the efficiency of decolorization improved as the catalyst dosage increased from 0.25 to 1 g/L and subsequently declined. The enhancement in decolorization effectiveness with a higher quantity of photocatalyst can be linked to the growing active surface area that facilitates the photocatalytic breakdown of organic dye. Conversely, an additional

increase in the quantity of suspended photocatalyst resulted in a rise in the solution's turbidity and scattering effects, leading to reduced penetration of visible light. This diminishes the photocatalyst's ability to generate OH• radicals. Moreover, at elevated concentrations, the photocatalyst nanoparticles tend to cluster, leading to a decrease in the number of active sites [22-24].

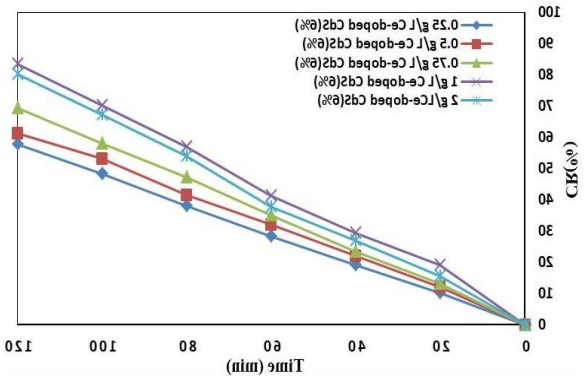

Figure 8. The effect of photocatalyst loading on the decolorization of 25 mg/L RB 19 by the $Ce_{0.06}Cd_{0.94}S$

3.2.5. Effect of different types of radical scavengers on the photocatalytic activity

The impact of various radical scavengers such as NaI, $Na_2S_2O_3$, Na_2CO_3, and 1, 4 Benzoquinone (BQ) was evaluated on the k_{app} of the photocatalytic reaction. Figure 9 illustrates the decolorization efficiency of RB 19 in the presence of inorganic ions including I^-, $S_2O_3^{2-}$, CO_3^{2-}, and $-OC_6H_4O$. The ions listed below capture the generated hydroxyl radicals as shown in Eqs. (7)– (12).

$I^-_{ads} + h^+_{ads} \rightarrow I^\bullet_{ads}$ (7)

$I^\bullet_{ads} + I^-_{ads} \rightarrow I^{\bullet-}_{ads}$ (8)

$HCO_3^-{}_{ads} + {}^\bullet OH_{ads} \rightarrow CO_3^{\bullet-} + H_2O$ (9)

$CO_3^{2-}{}_{ads} + {}^\bullet OH_{ads} \rightarrow CO_3^{\bullet-}{}_{ads} + OH^-$ (10)

$S_2O_3^{2-}{}_{ads} + {}^\bullet OH_{ads} \rightarrow S_2O_3^{\bullet-}{}_{ads} + OH^-$ (11)

$C_6H_4O_2 + {}^\bullet OH_{ads} \rightarrow {}^-OC_6H_4O^\bullet + OH^-$ (12)

The results are in good agreement with the published papers which reported a strong inhibiting effect of radical scavengers.

Additionally, the reactions mentioned indicate that the active sites on the CdS surface are obstructed by the generated radical anions, which are difficult to oxidize, leading to a reduction in photocatalytic activity. As a result, it can be inferred that RB 19 is initially taken up on the catalyst's surface and subsequently oxidized by the action of holes and hydroxyl radicals.

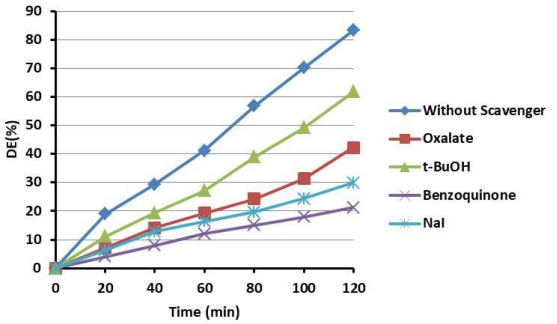

Figure 9. The effect of addition of I^-, CO^{3-}, $S_2O_3^{2-}$ ions and 1,4 Benzoquinone on the decolorization of 25 mg/L RB 19 ($Ce_{0.06}Cd_{0.94}S$ loading 0.1 g/L)

3.2.6. Reusability of the photocatalyst

The ability to be reused is a crucial aspect of a photocatalyst. Figure 10 displays the reusability assessments of the $Ce_{0.06}Cd_{0.94}S$ photocatalyst in the decolorization of RB 19 across 5 cycle experiments under ideal conditions, specifically: 25 mg/L of RB 19, 1 g/L of $Ce_{0.06}Cd_{0.94}S$ catalyst, and light exposure duration of 120 min. Following each decolorization experiment, the photocatalyst was rinsed with distilled water, dried at 50 °C for 3 hours, and subsequently utilized in a new experiment. As illustrated in Fig. 10, $Ce_{0.06}Cd_{0.94}S$ demonstrated remarkable chemical stability, with no considerable decomposition or photocorrosion observed over five cycles of photocatalytic reaction.

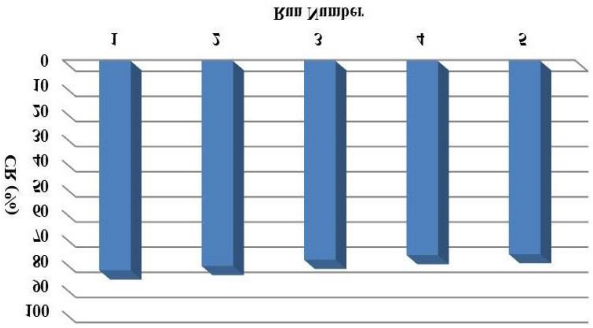

Figure 10. Reusability of the 6% Ce-doped CdS nanostructures within five consecutive experimental runs. $[RB\ 19]_0$ = 25 mg/L, $[Catalyst]_0$ = 1 g/L, and the reaction time = 120 min.

4. Conclusion

In this study, pure and cerium-doped CdS nanoparticles were successfully synthesized via a simple hydrothermal approach and employed as visible-light-responsive photocatalysts for the degradation of Reactive Blue 19 dye. Energy-dispersive X-ray spectroscopy confirmed the effective incorporation of

Ce ions into the CdS lattice, validating the successful doping process.

Comparative photocatalytic experiments revealed that Ce-doped CdS exhibited significantly higher decolorization efficiency than pure CdS, with the activity strongly dependent on cerium concentration. Among the tested samples, the optimized Ce content resulted in the most effective degradation performance. Investigation of radical scavengers—including iodide, carbonate, sulfite, and 1,4-benzoquinone—showed a marked decline in photocatalytic efficiency upon their addition, indicating the active involvement of reactive oxygen species in the reaction mechanism. Notably, 1,4-benzoquinone exerted the most pronounced inhibitory effect, underscoring the key role of superoxide radicals in the degradation pathway.

Overall, the findings demonstrate that Ce-doped CdS nanoparticles possess high photocatalytic activity and stability under visible light, making them promising and reusable catalysts for the effective removal of organic pollutants in wastewater treatment applications.

Competing interests

The authors declare no competing interests.

Acknowledgment

This work is funded by the Sayyed Jamaleddin Asadabadi University Research Grant.

References

[1] Khan A, Haque MM, Mir NA, Muneer M, Boxall C. Heterogeneous photocatalysed degradation of an insecticide derivative acetamiprid in aqueous suspensions of semiconductor. Desalination. 2010 Oct 15; 261(1-2):169-74. https://doi.org/10.1016/j.desal.2010.05.001

[2] Nitschke L, Schüssler W. Surface water pollution by herbicides from effluents of waste water treatment plants. Chemosphere. 1998 Jan 1; 36(1):35-41. https://doi.org/10.1016/S0045-6535(97)00286-5.

[3] Konstantinou IK, Sakkas VA, Albanis TA. Photocatalytic degradation of propachlor in aqueous TiO2 suspensions. Determination of the reaction pathway and identification of intermediate products by various analytical methods. Water research. 2002 Jun 1;36(11):2733-42. https://doi.org/10.1016/S0043-1354(01)00505-X

[4] Khataee AR, Aleboyeh H, Aleboyeh A. Crystallite phase-controlled preparation, characterisation and photocatalytic properties of titanium dioxide nanoparticles. Journal of Experimental Nanoscience. 2009 Jun 1; 4(2):121-37. https://doi.org/10. 1080/17458080902 929 945

[5] Khataee A, Khataee A, Fathinia M, Hanifehpour Y, Joo SW. Kinetics and mechanism of enhanced photocatalytic activity under visible light using synthesized Pr x Cd1–x Se nanoparticles. Industrial & Engineering Chemistry Research. 2013 Sep 18;52(37):13357-69. https://doi.org/10.1021/ie402352g.

[6] Hamnabard N, Hanifehpour Y, Khomami B, Joo SW. Synthesis, characterization and photocatalytic performance of Yb-doped CdTe nanoparticles. Materials Letters. 2015 Apr 15;145:253-7. https://doi.org/10.1016/j.matlet.2015.01.074.

[7] Roselin LS, Selvin R. Photocatalytic degradation of reactive orange 16 dye in a ZnO coated thin film flow photoreactor. Science of Advanced Materials. 2011 Apr 1; 3(2):251-8. https://doi.org/10.1166/sam.2011.1151.

[8] Hanifehpour Y, Mirtamizdoust B, Cheney MA, Joo SW. Facile synthesis, characterization and BET study of neodymium-doped spinel Mn 3 O 4 nanomaterial with enhanced photocatalytic activity. Journal of Materials Science: Materials in Electronics. 2017 Aug; 28:11654-64. https://doi.org/10.1007/s10854-017-6968-5.

[9] Hanifehpour Y, Hamnabard N, Mirtamizdoust B, Joo SW. Sonochemical synthesis, characterization and sonocatalytic performance of terbium-doped CdS nanoparticles. Journal of Inorganic and Organometallic Polymers and Materials. 2016 May;26(3):623-31. https://doi.org/10.1007/s10904-016-0352-4.

[10] Cheng L, Xiang Q, Liao Y, Zhang H. CdS-based photocatalysts. Energy & Environmental Science. 2018;11(6):1362-91. DOI https://doi.org/10.1039/C7EE03640J.

[11] Soltani N, Saion E, Hussein MZ, Erfani M, Abedini A, Bahmanrokh G, Navasery M, Vaziri P. Visible light-induced degradation of methylene blue in the presence of photocatalytic ZnS and CdS nanoparticles. International journal of molecular sciences. 2012 Sep 25;13(10):12242-58. https://doi.org/10.3390/ijms131012242.

[12] Arabzadeh A, Salimi A. One dimensional CdS nanowire@ TiO2 nanoparticles core-shell as high performance photocatalyst for fast degradation of dye pollutants under visible and sunlight irradiation. Journal of colloid and interface science. 2016 Oct 1;479:43-54. https://doi.org/10.1016/j.eti.2025.104061.

[13] Hanifehpour Y, Abdolmaleki M, Joo SW. Europium-doped Y2O3-coated diatomite nanomaterials: hydrothermal synthesis, characterization, optical study with enhanced photocatalytic performance. Inorganics. 2021 Dec 14;9(12):88. https://doi.org/10.3390/inorganics9120088

[14] Hanifehpour Y, Joo SW, Hamnabard N, Jung JH. The electrochemical performance and catalytic properties of Ytterbium substitution on Manganese oxide nanoparticles: BET study; preparation and characterization. Journal of Materials Science:

Materials in Electronics. 2019 Oct;30(20):18897-909. https://doi.org/10.1007/s10854-019-02246-4.
[15] Hanifehpour Y, Soltani B, Amani-Ghadim AR, Hedayati B, Khomami B, Joo SW. Synthesis and characterization of samarium-doped ZnS nanoparticles: A novel visible light responsive photocatalyst. Materials Research Bulletin. 2016 Apr 1;76:411-21. https://doi.org/10.1016/j. materresbull.2015.12.035
[16] Senthil K, Mangalaraj D, Narayandass SK. Structural and optical properties of CdS thin films. Applied surface science. 2001 Jan 15;169:476-9. https://doi.org/10.1016/S0169-4332(00)00732-7
[17] Singh V, Sharma PK, Chauhan P. Synthesis of CdS nanoparticles with enhanced optical properties. Materials Characterization. 2011 Jan 1;62(1):43-52. https://doi.org/10.1016/j .match ar. 2010.10.009.
[18] Khataee A, Bozorg S, Vahid B, Dang TD, Hanifehpour Y, Woo Joo S. Synthesis and Immobilization of MnO2 Nanoparticles on Bio-silica for the Efficient Degradation of an Azo Dye in the Aqueous Solution. Current Nanoscience. 2015 Feb 1;11(1):129-34. https://doi.org/10.2174/1573413710666140917211140
[19] Khataee A, Arefi-Oskoui S, Abdollahi B, Hanifehpour Y, Joo SW. Synthesis and characterization of $Pr_x Zn_{1-x} Se$ nanoparticles for photocatalysis of four textile dyes with different molecular structures. Research on Chemical Intermediates. 2015 Nov;41(11):8425-39. https://doi.org/10.1007/s11164-014-1901-5
[20] Mohamed RM, Harraz FA, Mkhalid IA. Hydrothermal synthesis of size-controllable Yttrium Orthovanadate (YVO4) nanoparticles and its application in photocatalytic degradation of direct blue dye. Journal of alloys and compounds. 2012 Aug 15; 532:55-60. https://doi.org/10.1016/j.jallcom.2012.04.016
[21] Khataee AR, Hosseini M, Hanifehpour Y, Safarpour M, Joo SW. Hydrothermal synthesis and characterization of Nd-doped ZnSe nanoparticles with enhanced visible light photocatalytic activity. Research on Chemical Intermediates. 2014 Feb;40(2):495-508. https://doi.org/10.1007/s11164-012-0977-z.
[22] Hanifehpour Y, Hamnabard N, Khomami B, Joo SW, Min BK, Jung JH. A novel visible-light Nd-doped CdTe photocatalyst for degradation of Reactive Red 43: synthesis, characterization, and photocatalytic properties. Journal of Rare Earths. 2016 Jan 1;34(1):45-54. https://doi.org/10.1016/S1002-0721(14)60576-7
[23] Hanifehpour Y, Soltani B, Amani-Ghadim AR, Hedayati B, Khomami B, Joo SW. Praseodymium-doped ZnS nanomaterials: Hydrothermal synthesis and characterization with enhanced visible light photocatalytic activity. Journal of industrial and engineering chemistry. 2016 Feb 25; 34:41-50. https://doi.org/10.1016/j.jiec.2015.10.032.
[24] Hanifehpour, Y., Rahmani, N., & Joo, S. W. (2024). Hydrothermal Synthesis of Terbium doped Antimony Selenide Nanomaterials and Investigation of Their Photocatalytic Performance. *Advances in Energy and Materials Research*, *1*(1), 23-28. doi: https://doi.org/10.22091/jaem.2023.9656.1005